**The Human Cytomegalovirus Tegument Protein pp65 (pUL83) Dampens Type I Interferon Production by Inactivating the DNA Sensor cGAS without Affecting STING [*Biolatti M, Dell'Oste V* co-first authors]**

# The Human Cytomegalovirus Tegument Protein pp65 (pUL83) Dampens Type I Interferon Production by Inactivating the DNA Sensor cGAS without Affecting STING

Matteo Biolatti,[a] Valentina Dell'Oste,[a] Sara Pautasso,[a] Francesca Gugliesi,[a] Jens von Einem,[b] Christian Krapp,[c] Martin Roelsgaard Jakobsen,[c] Cinzia Borgogna,[d] Marisa Gariglio,[d] Marco De Andrea,[a,d] and Santo Landolfo[a]#.

Department of Public Health and Pediatric Sciences, University of Turin, Turin, Italy[a]; Institute of Virology, University Medical Center Ulm, Ulm, Germany[b]; Department of Biomedicine, Aarhus University, Aarhus, Denmark[c]; Department of Translational Medicine, Novara Medical School, Novara, Italy[d].

Running Head: pp65/cGAS Interactome during HCMV Replication

#Address correspondence to Santo Landolfo, santo.landolfo@unito.it.

M.B. and V.D.O. contributed equally to this work.

Word count Abstract: 217

Word Count Text: 7015

## ABSTRACT

The innate immune response plays a pivotal role during human cytomegalovirus (HCMV) primary infection. Indeed, HCMV infection of primary fibroblasts rapidly triggers strong induction of type I interferons (IFN-I) accompanied by proinflammatory cytokine release. Here, we show that primary human foreskin fibroblasts (HFFs) infected with a mutant HCMV TB40/E strain unable to express UL83-encoded pp65 (v65Stop) produce significantly higher IFN-β levels than HFFs infected with the wild-type TB40/E strain or the pp65 revertant (v65Rev), suggesting that the tegument protein pp65 may dampen IFN-β production. To clarify the mechanisms through which pp65 inhibits IFN-β production, we analyzed the activation of the cGAS/STING/IRF3 axis in HFFs infected with either wild-type, v65Rev or the pp65-deficient mutant v65Stop. We found that pp65 selectively binds to cGAS and prevents its interaction with STING, thus inactivating the signaling pathway through the cGAS/STING/IRF3 axis. Consistently, addition of exogenous cGAMP to v65Rev infected cells triggered the production of IFN-β levels similar to those observed with v65Stop infected cells confirming that pp65 inactivation of IFN-β production occurs at the cGAS level. Notably, within the first 24 hours of HCMV infection, STING undergoes proteasome degradation independent of the presence or absence of pp65. Collectively, our data provide mechanistic insights into the interplay between HCMV pp65 and cGAS, leading to subsequent immune evasion by this prominent DNA virus.

48 **IMPORTANCE**

49 Primary human foreskin fibroblasts (HFFs) produce type I IFN (IFN-I) when infected with
50 HCMV. However, we observed significantly higher IFN-β levels when HFFs were infected with
51 HCMV unable to express UL83-encoded pp65 (v65Stop), suggesting that pp65 (pUL83) may
52 constitute a viral evasion factor. This study demonstrates that HCMV tegument protein pp65 inhibits
53 IFN-β production by binding and inactivating cGAS early during infection. In addition, this inhibitory
54 activity specifically targets cGAS since it can be bypassed via the addition of exogenous cGAMP, even
55 in presence of pp65. Notably, STING proteasome-mediated degradation was observed in both the
56 presence and absence of pp65. Collectively, our data underscore the important role of tegument protein
57 pp65 as a critical molecular hub in HCMV's evasion strategy to the innate immune response.
58
59
60
61
62
63
64
65
66
67
68
69
70
71

## INTRODUCTION

Human cytomegalovirus (HCMV), a member of the *Herpesviridae* family, is a widespread pathogen with a seroprevalence that ranges from 50% to 90% depending on geographical area and socioeconomic factors. The virus establishes a lifelong infection that is asymptomatic in the immunocompetent host despite occurrence of periodic reactivation and subsequent virus-shedding episodes. However, reactivation in the immunocompromised host or infection of the immunologically naïve fetus *in utero* can cause significant morbidity and mortality. Indeed, congenital HCMV infection can lead to abortion or dramatic disabilities, such as deafness and mental retardation (1, 2).

Pathogen recognition receptors (PRRs) detect viral components, such as viral nucleic acid, and subsequently lead to the induction of type I interferons (IFN-I), including IFN-α/β, which, in turn, triggers the expression of numerous IFN-stimulated genes (ISGs) (3). PRRs may be located either on the cell membrane, e.g. Toll-like receptors, or in the cytosol and in the nucleus; the latter group includes retinoic acid-inducible gene I (RIG-I)-like receptors, nucleotide-binding oligomerization domain (NOD)-like receptors, and several proteins involved in the DNA damage response (4–7). Intracellular dsDNA receptors, such as DNA-dependent activator of interferon regulatory factors (DAI; also known as ZBP1) (8, 9) and IFN-γ-inducible protein 16 (IFI16), have been identified to recognize HCMV components (10–16). More recent studies have demonstrated that the dsDNA receptor - cyclic GMP/AMP (cGAMP) synthase (cGAS) - is activated upon HCMV DNA binding and synthesizes the second messenger 2'-5'/3'-5' GMP/AMP (cGAMP) (17–21). Subsequently, cGAMP binds to the ER transmembrane adaptor protein stimulator of IFN genes (STING) and triggers its translocation from the ER to perinuclear punctate structures in order to induce IFN-I induction via TANK-binding kinase (TBK1) and IFN regulatory factor 3 (IRF3) (13, 22, 23).

On the opposing side, viruses have adopted various strategies to evade host innate immune responses and to establish persistent infection (14, 24–26). In particular, herpesviruses have evolved

strategies that target distinct steps in the signaling of IFN-I production (27–29). Su and Zheng (30) showed that HSV-1 tegument protein UL41 was involved in counteracting the cGAS/STING-mediated DNA-sensing pathway. HSV-1 ICP0, a viral E3 ubiquitin ligase, was shown to promote proteasome-dependent degradation of the DNA sensor IFI16 (31, 32). Another HSV-1 immediate early gene product, ICP27, has been demonstrated to antagonize IFN-I signaling by targeting the TBK1-activated STING signalosome, followed by accumulation of IRF3 into the nucleus (33), or by downregulating STAT-1 phosphorylation and accumulation in the nucleus (34). Finally, VP16, an abundant 65-kDa HSV-1 virion phosphoprotein, has been shown to inhibit IRF3 from recruiting its coactivator CREB-binding protein, thereby blocking its transactivation activity (35). With respect to HCMV, previous studies by Abate at al. (36) demonstrated that during virus infection pp65 prevented IRF3 activation in the IFN-I response by inhibiting its nuclear accumulation associated with a reduced IRF3 phosphorylation state. Moreover, pp65 has been shown to bind directly to the nuclear DNA sensor IFI16, which impairs its DNA-dependent oligomerization and triggers its nuclear delocalization followed by inhibition of subsequent immune signals (26, 37). Consistent with these results, another HCMV tegument protein, pUL82/pp71, was recently identified as a negative regulator of the STING-dependent antiviral response, impairing its cellular trafficking and formation of the TBK1/IRF3 complex (29).

Although these studies demonstrate that tegument proteins can down-regulate type I interferons production during HCMV infection, they currently offer only limited insight into the mechanisms these viral proteins rely on to counteract the cGAS/STING/IRF3 axis leading to reduced IFN-I production. Thus, to fill this gap, we sought to compare the IFN-β response in HFFs upon infection with a pp65 mutant HCMV, that is unable to express UL83-encoded pp65 (v65Stop), with that observed with the wild-type TB40/E strain (wild-type) or the pp65 revertant (v65Rev) viruses that express normal levels of pp65.

We show that primary HFFs infected with HCMV v65Stop produce significantly higher IFN-β levels than HFFs infected with HCMV wild-type or v65Rev, suggesting that the tegument protein pp65 impairs IFN-β production. Furthermore, when we analyzed the mode of action, we found that pp65 binds to cGAS and inhibits the release of a biologically active cGAMP, preventing its interaction with STING, and thus interfering with the cGAS/STING signaling pathway. The finding that the response to exogenous cGAMP is not affected by pp65 confirms that cGAS is the key target of pp65. Finally, we demonstrate that STING undergoes rapid degradation early during infection independent of pp65. Altogether, this work defines a previously unrecognized mechanism underlying HCMV evasion, i.e. cGAS inactivation, which assigns a critical role to pp65 in determining the outcome of host defense and viral pathogenesis.

## RESULTS

**The HCMV tegument protein pp65 inhibits IFN-β induction early during infection**. It has been demonstrated that infection of HFFs with HCMV induces the production of IFN-I through activation of the cGAS/STING/IRF3 signaling pathway (13, 21, 26, 29). On the opposing side, the HCMV tegument protein pp65 has been shown to inhibit IFN-I expression by preventing IRF3 activation or by inhibiting IFI16-mediated DNA sensing for immune evasion (36), suggesting that the cGAS/STING/IRF3 and/or IFI16-signaling pathways become blocked. Here we sought to determine whether the immunosuppressive function of pp65 could also be extended to other components of these signaling pathways, i.e. cGAS and STING, thereby interfering with the activation of IFN-I production. For this purpose, we compared IFN-β induction in HFFs infected with a pp65 mutant virus unable to express UL83-encoded pp65 (v65Stop), the TB40/E wild-type virus or the revertant (v65Rev) virus (37, 38). To this end, HFFs were mock-infected, infected with wild-type, v65Rev, or infected with v65Stop at an MOI of 1 and total RNA, harvested at 6 h post infection (hpi), was analyzed by RT-qPCR. As shown in

144 Fig. 1A, the IFN-β mRNA levels observed with v65Stop were ~2.7-fold higher than those observed
145 with wild-type- or v65Rev- virus-infected cells, suggesting that HCMV pp65 impairs IFN-β
146 production. Interestingly, HFF treatment with the synthetic dsRNA poly(I:C), which mimics RNA
147 virus infection and induces antiviral immune responses by promoting the production of both type I
148 IFNs (39), induced IFN-β levels similar to those observed in cells infected with v65Stop.

149 To provide further evidence supporting the physiological relevance of pp65 in the regulation of
150 IFN-β production, HFFs, transduced with an adenoviral-derived vector constitutively expressing pp65
151 protein (AdVpp65) or with control vector AdVLacZ at an MOI of 50 for 24 h, were infected with
152 v65Stop for 6 h (MOI of 1). RT-qPCR analysis revealed that IFN-β mRNA transcription was
153 significantly decreased in AdVpp65-infected cells compared with AdVLacZ-infected cells (~90%
154 reduction) (Fig. 1B). Taken together, these results support the immunosuppressive role of pp65 in
155 down-regulating IFN-β production in HCMV-infected cells and its contribution to innate immune
156 response evasion.

157 Next, we wanted to verify whether higher levels of IFN-β mRNA in v65Stop-infected HFFs
158 correlated with an increase in the production of biologically active IFN-β protein. To this purpose,
159 supernatants from HFFs infected with wild-type, v65Rev, and v65Stop viruses were harvested at 24 hpi
160 and assessed by ELISA for IFN-β production. In parallel, HFFs were stimulated with poly(I:C). As
161 shown in Fig. 1C, consistent with the results obtained with RT-qPCR, the levels of IFN-β secreted at
162 24 hpi were significantly higher when cells were infected with the v65Stop virus or stimulated with
163 poly(I:C), compared to those observed with HFFs infected with wild-type or v65Rev viruses,
164 confirming that in the presence of HCMV pp65 the transduction pathway leading to IFN-β production
165 is impaired (Fig. 1C).

166 **HCMV pp65 dampens IFN-β production by inactivating the cGAS/STING/IRF3 axis.** HCMV
167 infection can be detected by multiple innate sensing pathways, including TLR2 and TLR9, in diverse

cell types (14, 40, 41). In addition to TLRs, the HCMV dsDNA genome directly engages cytosolic or nuclear DNA-sensing pathways, including DAI/ZBP1 (42), AIM2 (43, 44), the cGAS/STING/IRF3 axis, and IFI16, respectively (13, 20, 21, 33, 39, 45–47).

To better understand how pp65 dampens IFN-β production during HCMV infection, we generated knockout (KO) gene variants in HFFs through CRISPR-Cas 9 technology. Primary cell lines carrying mutations in genes encoding cGAS (cGAS KO), STING (STING KO), and IFI16 (IFI16 KO) were generated based on three different guide RNAs. Verification of genetic KO was carried out by RT-qPCR, Western blot, and TIDE (Tracking of Indels by DEcomposition) analysis (48). As shown in Fig. 2, expression of cGAS, STING, and IFI16 genes was efficiently abrogated at both the mRNA (panel A) and protein (panel B) levels. Moreover, a TIDE analysis of the STING and IFI16 knockdown populations shows an overall knockdown efficiency of 87% (Fig. 2C) and 82% (Fig. 2D) respectively. This shows that in above 80% of the cells carry an indel (insertion or deletion) in the targeted gene, that leads to a frameshift in the reading frame, rendering the gene not-functional. Unfortunately, due to a technical limitation of the TIDE analysis, we have been so far unable to confirm cGAS knockout in CRISPR/Cas9 expressors. This limitation is likely due to the high number of repeats upstream and downstream the region of the cGAS gene (MB21D1) targeted by the gRNA, which makes it nearly impossible to generate a clean target side spanning PCR amplicon. Furthermore, this region displays an unusually high GC content, which, coupled with the high repeat number, is likely responsible for the low signal-to-noise ratio and the ensuing early sequencing termination that has hampered our attempts. However, the Western Blot and qPCR data clearly shows that the majority of the cells is silenced for cGAS (Fig. 2A, B).

We therefore sought to determine whether these KO cell lines exhibited a dependence on these three genes for HCMV-induced IFN-β expression. Consistent with the above results (Fig. 1), elevated IFN-β mRNA induction was observed at 6 hpi in normal HFFs infected with v65Stop, whereas

192 infection with wild-type virus or v65Rev virus triggered lower, albeit significant levels of IFN-β
193 mRNA expression. By contrast, induction of IFN-β mRNA expression was completely abolished in
194 HFFs lacking cGAS or STING independent of the type of virus used for infection. Interestingly,
195 although dramatically decreased, a minor residual of IFN-β induction was still observed in IFI16 KO
196 cells (Fig. 3A).

197 Taken together, these results confirm that cGAS and STING, and to a lesser extent IFI16, are
198 required for early immune activation by HCMV infection, consistent with the results reported by other
199 investigators (21, 49).

200 Next, to address whether disruption of the IFI16/cGAS/STING pathway affected the secretion
201 of IFN-β, we performed an ELISA specific for IFN-β using supernatants obtained from HFFs
202 permanently depleted for IFI16, cGAS, or STING, respectively, and then infected with wild-type,
203 v65Rev or v65Stop for 24 h. A significant decrease in IFN-β production was observed in cells depleted
204 for cGAS and STING and then infected with wild-type, v65Rev or v65Stop viruses (Fig. 3B), thus
205 confirming that these proteins are necessary for the effective production of IFN-β during HCMV
206 infection, independent of the presence of pp65. In agreement with the RT-qPCR results, a residual
207 induction of IFN-β release was observed in HCMV-infected IFI16-deficient compared with HFFs void
208 of cGAS and STING. Altogether, these results indicate that cGAS and STING, and to a lesser extent
209 IFI16, are essential to mount abundant IFN-β responses to HCMV.

210 To exclude potential off-target effects of the cGAS-, STING-, and IFI16-directed CRISPR
211 knockout, we assessed innate immune responses to the synthetic dsRNA poly(I:C), known to trigger
212 RIG-I activation (39). In this case, both IFN-β expression and release were not affected by knocking
213 out the above genes, thereby ruling out non-specific off-target effects (Fig. 3C, D).

214 **pp65 inhibits enzymatic activity of cGAS.** To define the relative role of cGAS and pp65 interplay in
215 innate sensing, we examined the production of cGAMP - the product of cGAS - in HFFs upon infection

with wild-type, v65Rev or v65Stop viruses. cGAMP activity was measured in cell extracts using a modified bioassay based on the original method of Orzalli et al. (50) that analyses the induction of IFN-β transcripts, as a marker of cGAMP activity, in permeabilized secondary reporter cells (HFFs) at 24 hpi. As shown in Fig. 4A, an increase in cGAMP activity was observed in HCMV-infected HFFs. However, the lack of pp65 in cells infected with v65Stop resulted in more robust cGAMP activity compared with wild-type and v65Rev-infected cells, indicating that interaction of pp65 with cGAS impairs cGAMP production.

To understand whether pp65 is able to modulate cGAMP activity by itself during viral replication, HFFs transfected with an HaloTag® fusion plasmid expressing the full-length pp65 (indicated as pp65 Halo-WT) were infected with HCMV v65Stop. At 6 hpi, the induction of IFN-β transcripts in permeabilized secondary reporter cells (HFFs) was measured (Fig. 4B). As expected, infection with v65Stop exhibited significantly higher cGAMP activity compared with mock-infected HFFs. Of note, the ability of v65Stop to induce IFN-β was almost completely ablated (~80%) after the expression of pp65 Halo-WT, further confirming that pp65 is crucial for cGAS activity suppression.

Next, we sought to determine whether the suppression exerted by pp65 was specific for HCMV DNA or could be extended to other cyclic di-nucleotides that are sensed by cGAS. Interestingly, a similar pattern of cGAMP activity modulation was observed following transfection of HFFs with the dsDNA synthetic analog poly(dA-dT), indicating that pp65 acts directly on cGAS activity, independently of the type of viral DNA, whether it is viral or synthetic (Fig. 4C).

As the DNA sensor IFI16 has been recently reported to cooperate with cGAS for DNA sensing in fibroblasts (50), human keratinocytes (46), and human macrophages (39), and to modulate STING activation in keratinocytes (46), we next tested whether IFI16 would be able to influence cGAS activity for the production of the second messenger cGAMP. To this purpose, cGAS KO, STING KO, and IFI16 KO HFFs (39) were infected with wild-type, v65Rev or v65Stop viruses, and whole-cell extracts

240 were harvested at 24 hpi and analyzed for the presence of cGAMP activity. As shown in Fig. 3D,
241 depletion of cGAS, STING, and IFI16 resulted in a significant reduction in IFN-β production,
242 confirming the cooperation of cGAS and IFI16 in cGAMP production upon HCMV infection.

243 Finally, to understand if the inhibitory activity of pp65 is limited to cGAS or could be extended
244 to downstream components of the cGAS/STING/IRF3 axis, we tested whether pp65 affects the
245 activation of STING by exogenous addition of cGAMP (39, 46). To this purpose, HFFs were
246 transfected with synthetic 2'3'-cGAMP or with the linearized 2'3'-cGAMP control, as described by
247 Jonsson et al. (39), Almine et al. (46), and the IFN-β gene expression response over time was
248 quantified. As shown in Fig. 4E, the delivery of synthetic cGAMP induced the expression of IFN-β
249 mRNA, peaking at 24 h post transfection (hpt), even in presence of pp65 Halo-WT, indicating that
250 pp65 inhibitory activity is limited to cGAS and can be bypassed by direct addition of 2'3'-cGAMP. As
251 expected, HFFs transfected with 2'3'-cGAMP control exhibited a severely blunted response.

252 **pp65 selectively interacts with cGAS.** To investigate whether cGAS localization could be regulated
253 during HCMV infection, HFFs were mock-infected or infected with wild-type, v65Rev or v65Stop
254 viruses (MOI of 1). The intracellular localization of pp65 and cGAS was assessed by confocal
255 microscopy at 2 hpi. In both mock- and HCMV-infected cells cGAS was localized in the cytoplasm, as
256 previously reported (27, 45, 51, 52). Interestingly, cGAS-defined puncta also occurred in the nucleus
257 (Fig. 5A), in accordance with Orzalli et al. (50), where they colocalized with pp65. Analysis of 3D
258 reconstructions created using the confocal Z stacks to enhance the colocalization analysis confirmed
259 this observation (Fig. 5A, far right pictures). Because pp65 and a subset of cGAS showed
260 colocalization, we hypothesized that they could form a heterocomplex. To learn more about the basis of
261 a pp65-cGAS interaction, we attempted to monitor the pp65-cGAS interaction during HCMV infection
262 *in situ* using a proximity ligation assay (PLA). PLA allows the detection of adjacent proteins through
263 the use of antibodies which recognize two proteins located within a maximum distance of 40 nm to

each other (37). Mock-, wild-type, v65Rev- and v65Stop-infected HFFs (MOI of 1) were fixed at 2 hpi, stained with anti-pp65 and anti-cGAS antibodies, and their interaction analyzed by PLA. As shown in Fig. 5B, cGAS and pp65 were mostly found in close proximity early on during HCMV infection with wild-type and v65Rev.

Given the novelty of these results, pp65-cGAS interaction was also confirmed by the immunoprecipitation (IP) of pp65 from lysates of infected cells at 2 hpi with an anti-pp65 monoclonal antibody (MAb), or with an unrelated MAb of the same isotype as negative control (CTRL). Immunoprecipitates were then analyzed by immunoblotting with antibodies directed against cGAS or pp65. The presence of pp65 and cGAS in all protein extracts was monitored by the analysis of Input control samples (non-immunoprecipitated whole-cell extracts) (Fig. 5C). As shown in Fig. 5C (left and middle panel), a band corresponding to cGAS was detectable in precipitates of wild-type and v65Rev-infected cell lysates when pp65 was precipitated with an antibody against virus pp65. The specificity of this interaction was verified by the observation that no signal was detected in immunoprecipitates obtained from v65Stop infected cell lysates (Fig. 4C, right panel) or in samples with CTRL antibody (Fig. 5C). Moreover, in coimmunoprecipitation experiments with STING, no interaction with pp65 could be observed (Fig. 5C), suggesting that pp65 interacts with cGAS, but not with STING during HCMV infection.

It has been demonstrated by our and other groups that pp65 binds to HCMV DNA (26, 37). DNA-binding proteins can associate during immunoprecipitation due to their adjacent binding on DNA rather than due to protein-protein interactions. To determine whether nucleic acid is required for the pp65/cGAS association, pp65 was immunoprecipitated from HCMV-infected cell lysates using anti-pp65 MAb in the presence or absence of the DNA-degrading enzyme benzonase, and then probed by Western blot analysis using an anti-cGAS antibody. cGAS was detected in immunoprecipitates from infected lysates in both the absence and presence of benzonase, whereas no migrating bands

288 corresponding to cGAS protein were detected in the absence of primary antibodies (Fig. 5D, left panel).
289 The activity of benzonase on nucleic acid was confirmed when the cell lysates analyzed in Fig. 4D
290 were examined on an ethidium bromide-stained agarose gel (Fig. 5D, right panel).

291 pp65 displays a bipartite structure, with a conserved N-terminal domain (~386 residues), a
292 divergent linker region, and a conserved C terminus (CTD, ~90 residues) (26). Thus, to learn more
293 about the basis of the pp65/cGAS interaction, we employed HaloTag® technology to generate
294 HaloTag® fusion plasmids expressing the full-length pp65 (indicated as pp65 Halo-WT), the N-
295 terminal domain (pp65 Halo-ΔC, deletion of residues 371-561), or the C-terminus (pp65 Halo-ΔN,
296 deletion of residues 1-414). HFFs were transfected with the above described constructs, and 72 h later,
297 IP was carried out using a MAb recognizing HaloTag, or control antibodies. Immunoprecipitated
298 proteins were examined by Western blot using antibodies recognizing cGAS. As depicted in Fig. 4E,
299 constructs harboring the N-terminal residues 1-414 could efficiently bind cGAS (Fig. 5E, lanes 1 and
300 3), while lack of this domain (lane 2) abolished cGAS binding. We can therefore conclude that the N-
301 terminal domain is necessary and sufficient for pp65 interaction with cGAS.

302 **pp65 does not interfere with STING proteasome degradation during HCMV infection.** Recent
303 work by Fu et al. (29) has shown that HCMV tegument protein pUL82/pp71 binds to and inhibits
304 STING-mediated signaling to evade innate antiviral immunity. To investigate whether pp65 could also
305 interfere with STING – the down-stream component of cGAS in the signaling pathway leading to IFN-
306 β production – we examined the levels of STING expression at different hpi in mock-infected HFFs, or
307 upon v65Rev- or v65Stop-infection (MOI of 1). As shown in Fig. 6A, cells infected with wild-type,
308 v65Rev and v65Stop viruses displayed comparable levels of cGAS up to 24 hpi that were similar to
309 those in mock HFFs. By contrast, infection with both v65Rev and v65Stop induced degradation of
310 STING within 24 hpi, suggesting that STING expression is independent of the presence of pp65.
311 Moreover, the finding that STING is activated in the first hours post transfection and then disappears

312 within 24 h in cells transfected with the synthetic dsDNA poly(dA-dT) (Fig. 6B) suggests that DNA
313 sensing, independent of pp65, is responsible for STING disappearance (29, 53–56).

314 We hypothesized that disappearance of STING before 24 hpi could be caused by a rapid
315 proteasomal degradation. To test this hypothesis, the effect of proteasomal inhibition on STING protein
316 levels was assessed early during HCMV infection. HFFs were pretreated with the proteasome inhibitor
317 MG132 for 30 min and then infected with either wild-type, v65Rev or v65Stop for 6 or 24 h. As shown
318 in Fig 6C, STING levels were rescued by MG132, in contrast to solvent-treated cells (DMSO),
319 indicating that STING undergoes proteasomal degradation early during HCMV infection.

320 To test whether ubiquitination is responsible for proteasomal degradation of STING as
321 previously reported (57), HFFs were infected with wild-type, v65Rev or v65Stop viruses (MOI of 1)
322 and ubiquitinated proteins immunoprecipitated from cell lysates by anti-ubiquitin antibodies followed
323 by detection of STING with specific anti-STING antibodies. As shown in Fig. 6D, upper panel, STING
324 was immunoprecipitated by anti-ubiquitin antibodies from HCMV infected cell lysates, suggesting that
325 HCMV infection induces ubiquitination and thus degradation of STING. K48-linked ubiquitination is
326 normally associated with proteasome-mediated protein degradation (57). By using a specific antibody
327 for immunoprecipitation and detection of STING in precipitates of HCMV infected cells, we confirm
328 the ubiquitination of STING on K48-linked residues that is apparently induced by HCMV infection
329 (Fig. 6E).

330

331 **DISCUSSION**

332 Viral DNA is recognized by various PRRs including DAI/ZBP1 (42), AIM2 (43, 44), IFI16,
333 and cGAS (13, 20, 21, 33, 39, 45–47). cGAS HCMV DNA sensing during the early phase of infection
334 that leads to the stimulation of the STING/TBK1/IRF3 signaling pathway followed by IFN production.
335 The IFN response antagonizes virus infection via the repression of viral replication, elimination of

336 virus-infected cells, and activation of adaptive immune responses (16, 20, 21, 52, 58, 59). On the
337 opposing side are diverse immune evasion strategies that viruses, including herpesviruses, have
338 evolved in order to inhibit the activation of PRRs, such as IFI16 and cGAS, and their down-stream
339 signaling cascades (60–64).

340 Although data are available on the activation of IFN production by HCMV, the mechanisms
341 HCMV relies on to counteract the cGAS signaling pathway are only partially defined. In order to fill
342 this gap, here we took advantage of three HCMV viruses: the wild-type TB40/E and the v65Rev, both
343 displaying intact pp65 expression capacity, and v65Stop, unable to express pp65 (38). Our data
344 demonstrate, for the first time, that the HCMV tegument protein pp65 directly binds and inhibits cGAS
345 enzymatic activity leading to down-regulation of IFN-β production (Fig. 7). The interaction of pp65
346 with cGAS required the presence of the N-terminal domain of pp65, whereas it appeared to be
347 independent of viral DNA, since the digestion of viral DNA by benzonase did not prevent protein
348 interaction, as shown by immunoprecipitation experiments. Consistent with this, addition of exogenous
349 cGAMP to v65Rev infected cells triggered the production of IFN levels similar to those observed with
350 v65Stop infected cells, confirming that pp65 inactivation of IFN-β production occurs at the cGAS
351 level. Thus, the functional relevance of the inhibitory activity of viral pp65 against cGAS can be
352 inferred by the observation that infection with a mutant virus that is unable to express pp65 results in a
353 significant increase in cGAS activity accompanied by a significant increase in IFN production.

354 Recent studies demonstrate that IFI16 and cGAS cooperate in the activation of STING during
355 the response to exogenous DNA sensing in human keratinocytes (46). In addition, it has been
356 demonstrated that IFI16 is required for early DNA sensing in human macrophages by promoting
357 cGAMP production (39). However, recent findings by Stetson's group (49) demonstrated that IFI16 is
358 not essential for the IFN response to human cytomegalovirus infection. Collectively, these results
359 indicate that the role of IFI16 in the IFN pathway is still a matter of debate. When we infected IFI16-

360 deficient HFFs, in an attempt to verify whether IFI16 also participates in the modulation of the IFN-β
361 response to HCMV, a residual IFN-β production was observed, compared to HFFs depleted of STING
362 and cGAS, suggesting that in human fibroblasts IFI16 is less involved in the signaling transduction
363 pathway leading to IFN production to HCMV. Partially consistent with our results, Paijo et al. (21)
364 demonstrated that HCMV- treated cGAS- or STING-deficient THP-1 monocytes exhibit significantly
365 impaired IFN-β production. In contrast, IFI16-deficient THP-1 monocytes infected with HCMV
366 mounted a robust IFN-β response that was moderately enhanced compared with that of wild-type THP-
367 1 cells. All these discrepancies might be explained by the different methods used to ablate IFI16 (i.e.,
368 CRISPR/Cas 9, siRNA, shRNA mediated IFI16 knock-down), by the different viruses and synthetic
369 DNA employed to stimulate the IFN-I response, and, finally, by the different target cell types employed
370 (i.e., HFFs, keratinocytes, monocytes, and plasmacytoid dendritic cells).

371 Having demonstrated that HCMV pp65 inhibits cGAS activation, next we investigated whether
372 pp65 could also inactivate STING, the downstream partner of cGAS. Recently, Fu et al. (29)
373 demonstrated that another HCMV tegument protein, namely pUL82/pp71, binds to and inhibits
374 STING-mediated signaling leading to viral innate immune evasion. Our results showed that pp65 does
375 not bind to STING and that regulation of its activity is independent of pp65, as its degradation is
376 observed within 24 hpi both in the presence or absence of the pp65 protein. This deduction was
377 generated from the following observations: i) STING degradation is observed upon infection with wild-
378 type, v65Rev or v65Stop: ii) immunoprecipitation experiments showed that pp65 doesn't bind to
379 STING; iii) STING degradation is also observed in the presence of unrelated dsDNA, such as synthetic
380 poly(dA-dT); and iv) it is not modulated by pp65. In addition, in the present study we report that
381 STING undergoes ubiquitination followed by degradation in HFFs infected with wild-type, v65Rev or
382 v65Stop within 6 h of infection. The following two findings led us to this conclusion: first,
383 pretreatment with MG132, a proteasome inhibitor, prevented STING degradation; second, STING was

ubiquitinated at Lys48, a marker of degradation by ubiquitination. Our results are consistent with previous studies that delineate the following model of STING activation and downstream signaling (Fig. 7): intracellular dsDNA induces autophagy and the trafficking of STING/TBK1 through the Golgi to endosomal compartments that harbor members of the IRF and NF-kB family. These transcription factors become activated and numerous immune-related genes are induced such as type I IFN and a variety of cytokines and chemokines. STING is then degraded and the signaling process halted. These events ensure the transient production of host defense genes required for direct antimicrobial effects as well as stimulating the adaptive immune response. Eventual suppression of STING function also ensures that the chronic production of cytokines is prevented, thus avoiding the consequences of inflammatory disease.

In conclusion, our data identify a previously unknown role of pp65 in down-regulating the cGAS/STING/IRF3 axis and thus IFN-β production (see proposed model in Fig. 7). The finding that HCMV, by means of its tegument proteins, i.e. pp65 and pUL82/pp71 interferes with the activity of all the components of this signaling pathway (i.e. cGAS, STING, and IRF3) in order to evade the IFN response underlines the relevance of the IFN system in blocking virus replication. Therefore, further delineation of the mechanisms through which HCMV inhibits cGAS/STING/IRF3 signaling will not only help our comprehension of this pathway, but may also facilitate the development of therapeutics aimed at ameliorating the diseases in which this pathway is altered.

## MATERIALS AND METHODS

**Cells and viruses.** Primary human foreskin fibroblasts (HFFs, ATCC SCRC-1041™), and human embryo kidney 293 cells (HEK 293) (Microbix Biosystems Inc.) were cultured in Dulbecco's modified Eagle's medium (DMEM) (Sigma-Aldrich) supplemented with 10% fetal calf serum (FCS) (Sigma-Aldrich) as previously described (39, 65). The HCMVs used in this study were all bacterial artificial

chromosome (BAC) clones. The clones of the endotheliotropic HCMV strain TB40/E wild-type, the revertant virus (v65Rev), and a mutant virus unable to express UL83-encoded pp65 (v65Stop) were previously generated (38). The viruses were propagated and titrated on HFFs and titrated by standard plaque assay (37, 66). HCMV infections were all performed at MOI of 1, where more than 50% of cells should be infected at 24 hpi (20, 38).

**Antibodies and reagents.** The following primary antibodies were used: rabbit polyclonal anti-cGAS (Sigma-Aldrich), anti-Ubiquitin-K48-specific (Millipore), anti-IFI16 (Santo Landolfo) or mouse monoclonal antibodies (MAb) anti-STING (R&D), anti-pp65 (Virusys), anti-HaloTag (Promega), anti-Vinculin (Sigma-Aldrich), and anti-α-Tubulin (Active-Motive). The following conjugated secondary antibodies were used: Alexa Fluor 488 anti-mouse or Alexa Fluor 568 anti-rabbit antibodies (Life Technologies) and horseradish peroxidase-labeled anti-mouse and anti-rabbit antibodies (GE Healthcare). The proteasome inhibitor MG132 (Calbiochem) was used at a concentration of 30 μM (67). Poly(dA-dT), and poly(I:C) (4 μg/mL, InvivoGen) (39, 68) were transfected into the cells using Lipofectamine 2000 according to the manufacturer's instructions (Life Technologies).

**Recombinant adenoviral vectors.** Adenovirus-derived vectors (AdV) expressing pp65 was generated by means of a replacement strategy using recombineering methods (69). Briefly, the UL83 ORF was amplified using specific set of primers (forward: AACCGTCAGATCGCCTGGAGACGCCATCCACGCTGTTTTGACCTCCATAGAAGACACCGG GACCGATCCAGCCTGGATCCATGGAGTCGCGCGGTCGCCG, reverse: TATAGAGTATACAATAGTGACGTGGGATCCCTACGTAGAATCAAGACCTAGGAGCGGGTT AGGGATTGGCTTACCAGCGCTACCTCGATGCTTTTTGGGC). In order to accomplish homologous recombination, approximately 200 ng of DNA derived from HCMV infected cells was electroporated into SW102 bacteria harboring pAdZ5-CV5 vectors. Cells were then plated on minimal medium agar plates containing 5% sucrose and chloramphenicol and incubated at 32°C for 1 day. The

colonies that appeared were inoculated into LB broth containing ampicillin and chloramphenicol and LB broth containing chloramphenicol only. In the colonies grown in chloramphenicol only, replacement of the UL83 ORF in multiple cloning sites and the ampicillin resistance were lost. Colonies were checked by PCR and sequencing. The AdVpp65 was cotransfected into HEK 293 cells. To obtain the recombinant adenoviruses, AdZ vectors were transfected into HEK 293 packaging cells. Transfected cells were maintained at 37°C with 5% $CO_2$ until an extensive cytopathic effect was obtained. Viruses were then purified from infected cultures by freeze-thaw-vortex cycles, and assessed for pp65 expression by Western blot. For cell transduction, HFFs were washed once with phosphate-buffered saline (PBS) and incubated with AdVpp65, at an MOI of 50 in DMEM. After 2 h at 37°C, the virus was washed off and fresh medium applied. For all the experiments, a recombinant adenovirus expressing the E. coli β-galactosidase gene (AdV-LacZ) was used as a control (66).

**Plasmid construction.** The HCMV UL83 sequences were amplified using specific sets of primers (pp65 Halo-WT forward: CGGAATTCATGGAGTCGCGCGGTCG, reverse: AACTCGAGACCTCGATGCTTTTTGGGCGT; pp65 Halo-ΔC forward: CGGAATTCATGGAGTCGCGCGGTCGCC, reverse: GCTCTAGAGGTGGTTACGAGTTCTTCGT; pp65 Halo-ΔN forward: GCGAATTCATGCAGTATCGCATCCAGGGCAAG, reverse: GCTCTAGAACCTCGATGCTTTTTGGGCGT). The 5′- and 3′- primers were engineered to contain EcoRI and XbaI restriction sites. The PCR fragments were subsequently digested and directionally cloned into the corresponding sites of the pHTC HaloTag® CMV-neo Vector (Promega). The following HaloTag fusion plasmids were constructed: plasmids expressing the full-length pp65 (indicated as pp65 Halo-WT), the N domain (pp65 Halo-ΔC, deletion between residues 371-561), or the C domain (pp65 Halo-ΔN, deletion between residues 1-414). Plasmids were then tested by Western blot and the nucleotide sequences confirmed by sequencing. HFFs were transiently transfected using a

455 MicroPorator (Digital Bio) according to the manufacturer's instructions (1200 V, 30 ms pulse width,
456 one impulse).

457 **RNA isolation and semiquantitative RT-qPCR.** Total RNA was extracted using the NucleoSpin
458 RNA kit (Macherey-Nagel) and 1 µg was retrotranscribed using the Revert-Aid H-Minus FirstStrand
459 cDNA Synthesis Kit (Fermentas), according to the manufacturer's protocol. Comparison of mRNA
460 expression between samples (i.e., infected versus untreated) was performed by SYBR green-based RT-
461 qPCR using Mx3000P apparatus (Stratagene), using the following primers: IFN-β forward
462 AAACTCATGAGCAGTCTGCA, IFN-β reverse AGGAGATCTTCAGTTTCGGAGG; the
463 housekeeping gene Glyceraldehyde-3-phosphate dehydrogenase (GAPDH) forward
464 AGTGGGTGTCGCTGTTGAAGT, GADPH reverse AACGTGTCAGTGGTGGACCTG.

465 **Transduction of HFFs with lentiviral CRISPR/Cas9.** The CRISPR/Cas9 system was employed to
466 generate specific gene knockouts in primary human fibroblasts. Specifically, we used a lentiviral
467 CRISPR/Cas9 vector54 that encodes a codon-optimized nuclear-localized Cas9 gene N-terminally
468 fused to the puromycin resistance gene via a T2A ribosome-skipping sequence. Additionally, the vector
469 contains a human U6 promoter driving expression of a guideRNA (gRNA) consisting of a gene-specific
470 CRISPR RNA (crRNA) fused to the trans-activating crRNA (tracrRNA) and a terminator sequence.
471 The gene-specific crRNA sequences cloned were: For IFI16 knockout 5'-
472 GTACCAACGCTTGAAGACC-3', for cGAS knockout 5'-GACTCGGTGGGATCCATCG-3' and for
473 STING knockout 5'-GAGCACACTCTC CGGTACC-3'.
474 VSVg-pseudotyped lenti-CRISPR virions were produced by transfecting HEK293T cells with the
475 following plasmids: CRISPR/Cas9 vector, pMD.2G, pRSV-REV, and pMDlg/p-RRE. Viral
476 supernatants were harvested after 72 h and used to transduce fibroblasts by infection in the presence of
477 4 mg/ml polybrene. Transduced cells were selected with increasing dosage of puromycin (from 0.5
478 µg/ml, 1 µg/ml and 2 µg/ml) over the course of 14 days post transduction. After selection the

479 successful knockout was confirmed using qPCR and immunoblotting. Additionally, indel frequencies
480 were quantified using TIDE (48); genomic DNA was extracted and PCR amplicons spanning the
481 sgRNA target site were generate. Purified PCR products were then Sanger-sequenced and Indel
482 frequencies quantified using the TIDE software (http://tide.nki.nl). A reference sequence (WT cells)
483 was used as a control.

484 **Immunofluorescence microscopy.** Indirect immunofluorescence analysis (IIF) was performed as
485 previously described (12) using the appropriate dilution of primary antibodies for 1 h at room
486 temperature (RT), followed by 1 h with secondary antibodies in the dark at RT. Nuclei were
487 counterstained with 4',6-diamidino-2-phenylindole (DAPI) or TO-PRO-3. Finally, coverslips were
488 mounted with Vectashield mounting medium (VECTOR). Samples were observed using a fluorescence
489 microscope (Olympus IX70) equipped with cellSens Standard - Microscopy Imaging Software, or a
490 confocal microscope (Leica TCS SP2). ImageJ software was used for image processing.

491 **Proximity ligation assay (PLA).** Proximity ligation assay (DuoLink, Sigma-Aldrich) was performed
492 using the DuoLink PLA Kit to detect protein–protein interactions using fluorescence microscopy
493 according to the manufacturer's protocol. Briefly, HFFs were infected with wild-type, v65Rev or
494 v65Stop viruses at an MOI of 1 for 2 h, fixed for 15 min at RT, permeabilized with 0.2% Triton X-100,
495 and blocked with 10% HCMV-negative human serum for 30 minutes at RT. Cells were then incubated
496 with primary antibodies diluted in TBS-Tween 0.05% for 1 h, washed, and then further incubated for
497 another hour at 37°C with species-specific PLA probes under hybridization conditions and in the
498 presence of 2 additional oligonucleotides to facilitate the hybridization only in close proximity (~40
499 nm). A ligase was then added to join the two hybridized oligonucleotides, thus forming a closed circle.
500 Using the ligated circle as template, rolling-circle amplification was initiated by adding an
501 amplification solution, generating a concatemeric product extending from the oligonucleotide arm of
502 the PLA probe. Lastly, a detection solution consisting of fluorophore-labeled oligonucleotides was

503 added, and the labeled oligonucleotides were hybridized to the concatemeric products. The signal was
504 detected as distinct fluorescent dots in the Texas Red channel and analyzed by fluorescence microscopy
505 (Olympus IX70). Negative controls consisted of mock-infected cells that were otherwise treated in the
506 same way as described for infected cells.

507 **Western blot analysis.** Whole-cell protein extracts were prepared and subject to Western blot analysis
508 as previously described (12, 70). Briefly, an equal amount of cell extracts were fractionated by
509 electrophoresis on sodium dodecyl sulfate polyacrylamide gels and transferred to Immobilon-P
510 membranes (Biorad). After blocking with 5% nonfat dry milk in TBS-Tween 0.05%, membranes were
511 incubated overnight at 4°C with the appropriate primary antibodies. Membranes were then washed and
512 incubated for 1 h at room temperature with secondary antibodies. Proteins were detected using an
513 enhanced chemiluminescence detection kit (SuperSignal West Pico Chemiluminescent Substrate,
514 Thermo SCIENTIFIC).

515 **Immunoprecipitation Assay.** Uninfected or HCMV-infected cells (MOI of 1) were washed with PBS
516 and lysed in radioimmunoprecipitation assay (RIPA) buffer (50 mM Tris pH 7.4; 150 mM NaCl; 1 mM
517 EDTA; 1% Nonidet P-40; 0.1% SDS; 0.5% deoxycholate; protease inhibitors). Two hundred
518 micrograms of proteins were incubated with 2 µg of specific antibody, or without antibody as negative
519 control, for 1 h at RT with rotation followed by an overnight incubation at 4°C with protein G–
520 Sepharose (Sigma-Aldrich). Immune complexes were collected by centrifugation and washed with
521 RIPA buffer. The Sepharose beads were pelleted and washed three times with RIPA buffer,
522 resuspended in reducing sample buffer (50 mM Tris pH 6.8; 10% glycerol; 2% SDS; 1% 2-
523 mercaptoethanol), boiled for 5 min, and resolved on a SDS-PAGE gel to assess protein binding by
524 Western blot. Where indicated, ~1 U/µL Benzonase (Sigma-Aldrich) was added for 2 h on ice as
525 described in Wu et al. (27). Immunoprecipitation of ubiquitin-conjugated proteins was performed using
526 the UbiQapture-Q Kit (Enzo LifeScience). A total of 25 µg of lysates from cultured cells were used per

assay. Samples were added to the tubes containing 20 µL UbiQapture-Q matrix and incubated for 3h at 4°C in a horizontal rotor mixer. The matrix was then carefully washed and the ubiquitin-protein conjugates were eluted by addition of 50 µL sample buffer and heating at 95°C for 10 min. The eluted fraction was clarified from the matrix and analyzed by immunoblotting.

**ELISA assay.** The IFN-β secreted in culture supernatants was analyzed using Single Analyte Human ELISA kits for IFN-β (Human IFN Beta ELISA KIT, PBL Assay Science) according to the manufacturer's instructions. All absorbance readings were measured at 450 nm using a Victor X4 Multilabel Plate Reader (Perkin Elmer).

**cGAMP activity assay.** cGAMP activity assay was performed as previously described (50, 52). Briefly, HFFs were infected with wild-type, v65Rev, v65Stop or transfected with poly(dA-dT) (4 µg/mL) (InvivoGen) or pp65 Halo-WT using Lipofectamine 2000 according to the manufacturer's instructions (Life Technologies). At the indicated times, cells were washed with PBS and lysed in hypotonic buffer (10 mM Tris pH 7.4; 10 mM KCl; 1.5 mM $MgCl_2$). Cell extracts were incubated with ~1 U/µL Benzonase (Sigma-Aldrich) for 30 min at 37°C. Cell extracts were then heated at 95°C for 5 min and centrifuged for 5 min at maximum speed (16,100 × g) in an Eppendorf microcentrifuge. HFFs were used as reporter cells to measure cGAMP production. HFFs were permeabilized as previously described (71) with modifications. Briefly, media was aspirated from the HFFs and digitonin permeabilization solution (50 mM Hepes pH 7.0, 100 mM KCl, 85 mM sucrose, 3 mM $MgCl_2$, 0.2% BSA, 1 mM ATP, 0.1 mM DTT, and 10 µg/mL digitonin) was added to treated cell extracts. HFF reporter cells were incubated with extracts for 30 min at 37 °C and then replaced with supplemented media. RNA was harvested 6 h after the initial addition of extracts and RT-qPCR for IFN-β, as a marker of cGAMP activity, and GADPH, as housekeeping gene, was performed as described above.

**Response to exogenous cGAMP.** Synthetic 2'3'-cGAMP (2 µg/mL, InvivoGen) or 2'3'-cGAMP control (2 µg/mL, InvivoGen), also known as 2'5'-GpAp, a linear dinucleotide analog after hydrolysis

of 2'3'-cGAMP by phosphodiesterases, were transfected into HFFs using Lipofectamine 2000 according to the manufacturer's instructions (Life Technologies). At the indicated time points, RNA was harvested and the IFN-β gene expression response quantified over time by RT-qPCR.

**Statistical analysis.** All statistical tests were performed using GraphPad Prism version 5.00 for Windows (GraphPad Software, San Diego California USA, www.graphpad.com). The data were presented as means ± standard deviations (SD). For comparisons consisting of two groups, means were compared using two-tailed Student's t-tests; for comparisons consisting of three groups, means were compared using one-way or two-way analysis of variance (ANOVA) with Bonferroni's post-tests. Differences were considered statistically significant for $P<0.05$ (*, $P<0.05$; **, $P<0.01$; ***, $P<0.001$).

**ACKNOWLEDGEMENTS**

This study was supported by: Italian Ministry of Education, University and Research - MIUR (PRIN 2015 to MDA, 2015W729WH; PRIN 2015 to VDO, 2015RMNSTA); Research Funding from the University of Turin 2017 to MDA, SL, and VDO; Regione Piemonte (Italy) (PAR-FCS 2007/2013) to SL; Compagnia di San Paolo (CSP 2014) to CB; Associazione Italiana per la Ricerca sul Cancro (AIRC) (IG 2016) to MG; Danish Council for Independent Research (4183-00275B) to MRJ and CK.

**REFERENCES**

1. Britt WJ. 2017. Congenital Human Cytomegalovirus Infection and the Enigma of Maternal Immunity 91 doi: 10.1128/JVI.02392-16.
2. Griffiths P, Baraniak I, Reeves M. 2015. The pathogenesis of human cytomegalovirus. J Pathol 235:288–297.
3. McNab F, Mayer-Barber K, Sher A, Wack A, O'Garra A. 2015. Type I interferons in infectious disease. Nat Rev Immunol 15:87–103.

4. Luecke S, Paludan SR. 2017. Molecular requirements for sensing of intracellular microbial nucleic acids by the innate immune system. Cytokine 98:4–14.

5. Dempsey A, Bowie AG. 2015. Innate immune recognition of DNA: A recent history. Virology 479–480:146–152.

6. Komatsu T, Nagata K, Wodrich H. 2016. The Role of Nuclear Antiviral Factors against Invading DNA Viruses: The Immediate Fate of Incoming Viral Genomes. Viruses 8 doi:10.3390/v8100290.

7. Zevini A, Olagnier D, Hiscott J. 2017. Crosstalk between Cytoplasmic RIG-I and STING Sensing Pathways. Trends Immunol 38:194–205.

8. Takaoka A, Wang Z, Choi MK, Yanai H, Negishi H, Ban T, Lu Y, Miyagishi M, Kodama T, Honda K, Ohba Y, Taniguchi T. 2007. DAI (DLM-1/ZBP1) is a cytosolic DNA sensor and an activator of innate immune response. Nature 448:501–505.

9. Upton JW, Kaiser WJ, Mocarski ES. 2012. DAI/ZBP1/DLM-1 complexes with RIP3 to mediate virus-induced programmed necrosis that is targeted by murine cytomegalovirus vIRA. Cell Host Microbe 11:290–297.

10. Li T, Diner BA, Chen J, Cristea IM. 2012. Acetylation modulates cellular distribution and DNA sensing ability of interferon-inducible protein IFI16. Proc Natl Acad Sci U S A 109:10558–10563.

11. Horan KA, Hansen K, Jakobsen MR, Holm CK, Søby S, Unterholzner L, Thompson M, West JA, Iversen MB, Rasmussen SB, Ellermann-Eriksen S, Kurt-Jones E, Landolfo S, Damania B, Melchjorsen J, Bowie AG, Fitzgerald KA, Paludan SR. 2013. Proteasomal degradation of herpes simplex virus capsids in macrophages releases DNA to the cytosol for recognition by DNA sensors. J Immunol Baltim Md 1950 190:2311–2319.

12. Dell'Oste V, Gatti D, Gugliesi F, De Andrea M, Bawadekar M, Lo Cigno I, Biolatti M, Vallino M, Marschall M, Gariglio M, Landolfo S. 2014. Innate nuclear sensor IFI16 translocates into the

cytoplasm during the early stage of in vitro human cytomegalovirus infection and is entrapped in the egressing virions during the late stage. J Virol 88:6970–6982.

13. Diner BA, Lum KK, Toettcher JE, Cristea IM. 2016. Viral DNA Sensors IFI16 and Cyclic GMP-AMP Synthase Possess Distinct Functions in Regulating Viral Gene Expression, Immune Defenses, and Apoptotic Responses during Herpesvirus Infection. mBio 7:e01553-16.
14. Orzalli MH, Knipe DM. 2014. Cellular Sensing of Viral DNA and Viral Evasion Mechanisms. Annu Rev Microbiol 68:477–492.
15. Knipe DM. 2015. Nuclear Sensing of Viral DNA, Epigenetic Regulation of Herpes Simplex Virus Infection, and Innate Immunity. Virology 0:153–159.
16. Diner BA, Lum KK, Cristea IM. 2015. The Emerging Role of Nuclear Viral DNA Sensors. J Biol Chem 290:26412–26421.
17. Sun L, Wu J, Du F, Chen X, Chen ZJ. 2013. Cyclic GMP-AMP synthase is a cytosolic DNA sensor that activates the type I interferon pathway. Science 339:786–791.
18. Gao P, Ascano M, Wu Y, Barchet W, Gaffney BL, Zillinger T, Serganov AA, Liu Y, Jones RA, Hartmann G, Tuschl T, Patel DJ. 2013. Cyclic [G(2′,5′)pA(3′,5′)p] Is the Metazoan Second Messenger Produced by DNA-Activated Cyclic GMP-AMP Synthase. Cell 153:1094–1107.
19. Bhat N, Fitzgerald KA. 2014. Recognition of cytosolic DNA by cGAS and other STING-dependent sensors. Eur J Immunol 44:634–640.
20. Lio C-WJ, McDonald B, Takahashi M, Dhanwani R, Sharma N, Huang J, Pham E, Benedict CA, Sharma S. 2016. cGAS-STING Signaling Regulates Initial Innate Control of Cytomegalovirus Infection. J Virol 90:7789–7797.
21. Paijo J, Döring M, Spanier J, Grabski E, Nooruzzaman M, Schmidt T, Witte G, Messerle M, Hornung V, Kaever V, Kalinke U. 2016. cGAS Senses Human Cytomegalovirus and Induces Type I Interferon Responses in Human Monocyte-Derived Cells. PLoS Pathog 12:e1005546.

622 22. Burdette DL, Monroe KM, Sotelo-Troha K, Iwig JS, Eckert B, Hyodo M, Hayakawa Y, Vance
623 RE. 2011. STING is a direct innate immune sensor of cyclic di-GMP. Nature 478:515–518.
624 23. Ishikawa H, Ma Z, Barber GN. 2009. STING regulates intracellular DNA-mediated, type I
625 interferon-dependent innate immunity. Nature 461:788–792.
626 24. Christensen MH, Paludan SR. 2017. Viral evasion of DNA-stimulated innate immune responses.
627 Cell Mol Immunol 14:4–13.
628 25. Ma Z, Damania B. 2016. The cGAS-STING Defense Pathway and Its Counteraction by Viruses.
629 Cell Host Microbe 19:150–158.
630 26. Li T, Chen J, Cristea IM. 2013. Human cytomegalovirus tegument protein pUL83 inhibits IFI16-
631 mediated DNA sensing for immune evasion. Cell Host Microbe 14:591–599.
632 27. Wu J, Li W, Shao Y, Avey D, Fu B, Gillen J, Hand T, Ma S, Liu X, Miley W, Konrad A, Neipel
633 F, Stürzl M, Whitby D, Li H, Zhu F. 2015. Inhibition of cGAS DNA Sensing by a Herpesvirus
634 Virion Protein. Cell Host Microbe 18:333–344.
635 28. Crow MS, Lum KK, Sheng X, Song B, Cristea IM. 2016. Diverse mechanisms evolved by DNA
636 viruses to inhibit early host defenses. Crit Rev Biochem Mol Biol 51:452–481.
637 29. Fu Y-Z, Su S, Gao Y-Q, Wang P-P, Huang Z-F, Hu M-M, Luo W-W, Li S, Luo M-H, Wang Y-Y,
638 Shu H-B. 2017. Human Cytomegalovirus Tegument Protein UL82 Inhibits STING-Mediated
639 Signaling to Evade Antiviral Immunity. Cell Host Microbe 21:231–243.
640 30. Su C, Zheng C. 2017. Herpes Simplex Virus 1 Abrogates cGAS/STING-Mediated Cytosolic
641 DNA-sensing Pathway via Its Virion Host Shutoff Protein UL41. J Virol doi:10.1128/JVI.02414-
642 16.
643 31. Orzalli MH, DeLuca NA, Knipe DM. 2012. Nuclear IFI16 induction of IRF-3 signaling during
644 herpesviral infection and degradation of IFI16 by the viral ICP0 protein. Proc Natl Acad Sci U S
645 A 109:E3008-3017.

646 32. Orzalli MH, Broekema NM, Knipe DM. 2016. Relative Contributions of Herpes Simplex Virus 1
647 ICP0 and vhs to Loss of Cellular IFI16 Vary in Different Human Cell Types. J Virol 90:8351–
648 8359.
649 33. Christensen MH, Jensen SB, Miettinen JJ, Luecke S, Prabakaran T, Reinert LS, Mettenleiter T,
650 Chen ZJ, Knipe DM, Sandri-Goldin RM, Enquist LW, Hartmann R, Mogensen TH, Rice SA,
651 Nyman TA, Matikainen S, Paludan SR. 2016. HSV-1 ICP27 targets the TBK1-activated STING
652 signalsome to inhibit virus-induced type I IFN expression. EMBO J 35:1385–1399.
653 34. Johnson KE, Song B, Knipe DM. 2008. Role for herpes simplex virus 1 ICP27 in the inhibition of
654 type I interferon signaling. Virology 374:487–494.
655 35. Xing J, Ni L, Wang S, Wang K, Lin R, Zheng C. 2013. Herpes simplex virus 1-encoded tegument
656 protein VP16 abrogates the production of beta interferon (IFN) by inhibiting NF-κB activation
657 and blocking IFN regulatory factor 3 to recruit its coactivator CBP. J Virol 87:9788–9801.
658 36. Abate DA, Watanabe S, Mocarski ES. 2004. Major Human Cytomegalovirus Structural Protein
659 pp65 (ppUL83) Prevents Interferon Response Factor 3 Activation in the Interferon Response. J
660 Virol 78:10995–11006.
661 37. Biolatti M, Dell'Oste V, Pautasso S, von Einem J, Marschall M, Plachter B, Gariglio M, De
662 Andrea M, Landolfo S. 2016. Regulatory Interaction between the Cellular Restriction Factor
663 IFI16 and Viral pp65 (pUL83) Modulates Viral Gene Expression and IFI16 Protein Stability. J
664 Virol 90:8238–8250.
665 38. Chevillotte M, Landwehr S, Linta L, Frascaroli G, Lüske A, Buser C, Mertens T, von Einem J.
666 2009. Major tegument protein pp65 of human cytomegalovirus is required for the incorporation of
667 pUL69 and pUL97 into the virus particle and for viral growth in macrophages. J Virol 83:2480–
668 2490.

669 39. Jønsson KL, Laustsen A, Krapp C, Skipper KA, Thavachelvam K, Hotter D, Egedal JH, Kjolby
670 M, Mohammadi P, Prabakaran T, Sørensen LK, Sun C, Jensen SB, Holm CK, Lebbink RJ,
671 Johannsen M, Nyegaard M, Mikkelsen JG, Kirchhoff F, Paludan SR, Jakobsen MR. 2017. IFI16
672 is required for DNA sensing in human macrophages by promoting production and function of
673 cGAMP. Nat Commun 8:14391 doi: 10.1038/ncomms14391.
674 40. Rathinam VAK, Fitzgerald KA. 2011. Innate immune sensing of DNA viruses. Virology
675 411:153–162.
676 41. Thompson MR, Kaminski JJ, Kurt-Jones EA, Fitzgerald KA. 2011. Pattern recognition receptors
677 and the innate immune response to viral infection. Viruses 3:920–940.
678 42. DeFilippis VR, Alvarado D, Sali T, Rothenburg S, Früh K. 2010. Human cytomegalovirus
679 induces the interferon response via the DNA sensor ZBP1. J Virol 84:585–598.
680 43. Huang Y, Ma D, Huang H, Lu Y, Liao Y, Liu L, Liu X, Fang F. 2017. Interaction between
681 HCMV pUL83 and human AIM2 disrupts the activation of the AIM2 inflammasome. Virol J 14
682 doi: 10.1186/s12985-016-0673-5.
683 44. Huang Y, Liu L, Ma D, Liao Y, Lu Y, Huang H, Qin W, Liu X, Fang F. 2017. Human
684 cytomegalovirus triggers the assembly of AIM2 inflammasome in THP-1-derived macrophages. J
685 Med Virol doi: 10.1002/jmv.24846.
686 45. Xia P, Wang S, Gao P, Gao G, Fan Z. 2016. DNA sensor cGAS-mediated immune recognition.
687 Protein Cell 7:777–791.
688 46. Almine JF, O'Hare CAJ, Dunphy G, Haga IR, Naik RJ, Atrih A, Connolly DJ, Taylor J, Kelsall
689 IR, Bowie AG, Beard PM, Unterholzner L. 2017. IFI16 and cGAS cooperate in the activation of
690 STING during DNA sensing in human keratinocytes. Nat Commun 8:14392.
691 47. Thompson MR, Sharma S, Atianand M, Jensen SB, Carpenter S, Knipe DM, Fitzgerald KA, Kurt-
692 Jones EA. 2014. Interferon γ-inducible protein (IFI) 16 transcriptionally regulates type i

693 interferons and other interferon-stimulated genes and controls the interferon response to both
694 DNA and RNA viruses. J Biol Chem 289:23568–23581.
695 48. Brinkman EK, Chen T, Amendola M, van Steensel B. 2014. Easy quantitative assessment of
696 genome editing by sequence trace decomposition. Nucleic Acids Res 42:e168.
697 49. Gray EE, Winship D, Snyder JM, Child SJ, Geballe AP, Stetson DB. 2016. The AIM2-like
698 Receptors Are Dispensable for the Interferon Response to Intracellular DNA. Immunity 45:255–
699 266.
700 50. Orzalli MH, Broekema NM, Diner BA, Hancks DC, Elde NC, Cristea IM, Knipe DM. 2015.
701 cGAS-mediated stabilization of IFI16 promotes innate signaling during herpes simplex virus
702 infection. Proc Natl Acad Sci U S A 112:E1773-1781.
703 51. Sun L, Wu J, Du F, Chen X, Chen ZJ. 2013. Cyclic GMP-AMP Synthase Is a Cytosolic DNA
704 Sensor That Activates the Type I Interferon Pathway. Science 339:786–791.
705 52. Gao D, Wu J, Wu Y-T, Du F, Aroh C, Yan N, Sun L, Chen ZJ. 2013. Cyclic GMP-AMP Synthase
706 Is an Innate Immune Sensor of HIV and Other Retroviruses. Science 341:903–906.
707 53. Liu Y, Li J, Chen J, Li Y, Wang W, Du X, Song W, Zhang W, Lin L, Yuan Z. 2015. Hepatitis B
708 Virus Polymerase Disrupts K63-Linked Ubiquitination of STING To Block Innate Cytosolic
709 DNA-Sensing Pathways. J Virol 89:2287–2300.
710 54. Wang Y, Lian Q, Yang B, Yan S, Zhou H, He L, Lin G, Lian Z, Jiang Z, Sun B. 2015. TRIM30α
711 Is a Negative-Feedback Regulator of the Intracellular DNA and DNA Virus-Triggered Response
712 by Targeting STING. PLOS Pathog 11:e1005012.
713 55. Castillo Ramirez JA, Urcuqui-Inchima S. 2015. Dengue Virus Control of Type I IFN Responses:
714 A History of Manipulation and Control. J Interferon Cytokine Res Off J Int Soc Interferon
715 Cytokine Res 35:421–430.

716 56. Kalamvoki M, Roizman B. 2014. HSV-1 degrades, stabilizes, requires, or is stung by STING
717 depending on ICP0, the US3 protein kinase, and cell derivation. Proc Natl Acad Sci U S A
718 111:E611-617.
719 57. Davis ME, Gack MU. 2015. Ubiquitination in the antiviral immune response. Virology 479–
720 480:52–65.
721 58. Ablasser A. 2016. ReGLUation of cGAS. Nat Immunol 17:347–349.
722 59. Paludan SR. 2015. Activation and regulation of DNA-driven immune responses. Microbiol Mol
723 Biol Rev MMBR 79:225–241.
724 60. Diner BA, Cristea IM. 2015. Blowing Off Steam: Virus Inhibition of cGAS DNA Sensing. Cell
725 Host Microbe 18:270–272.
726 61. Chan YK, Gack MU. 2016. Viral evasion of intracellular DNA and RNA sensing. Nat Rev
727 Microbiol 14:360–373.
728 62. Su C, Zhan G, Zheng C. 2016. Evasion of host antiviral innate immunity by HSV-1, an update.
729 Virol J 13:38 doi: 10.1186/s12985-016-0495-5.
730 63. Dell'Oste V, Gatti D, Giorgio AG, Gariglio M, Landolfo S, De Andrea M. 2015. The interferon-
731 inducible DNA-sensor protein IFI16: a key player in the antiviral response. New Microbiol 38:5–
732 20.
733 64. Landolfo S, De Andrea M, Dell'Oste V, Gugliesi F. 2016. Intrinsic host restriction factors of
734 human cytomegalovirus replication and mechanisms of viral escape. World J Virol 5:87–96.
735 65. Pignoloni B, Fionda C, Dell'Oste V, Luganini A, Cippitelli M, Zingoni A, Landolfo S, Gribaudo
736 G, Santoni A, Cerboni C. 2016. Distinct Roles for Human Cytomegalovirus Immediate Early
737 Proteins IE1 and IE2 in the Transcriptional Regulation of MICA and PVR/CD155 Expression. J
738 Immunol Baltim Md 1950 197:4066–4078.

739 66. Gariano GR, Dell'Oste V, Bronzini M, Gatti D, Luganini A, De Andrea M, Gribaudo G, Gariglio
740 M, Landolfo S. 2012. The intracellular DNA sensor IFI16 gene acts as restriction factor for
741 human cytomegalovirus replication. PLoS Pathog 8:e1002498.
742 67. Zhang Z, Evers DL, McCarville JF, Dantonel J-C, Huong S-M, Huang E-S. 2006. Evidence that
743 the human cytomegalovirus IE2-86 protein binds mdm2 and facilitates mdm2 degradation. J Virol
744 80:3833–3843.
745 68. Abe T, Barber GN. 2014. Cytosolic-DNA-mediated, STING-dependent proinflammatory gene
746 induction necessitates canonical NF-κB activation through TBK1. J Virol 88:5328–5341.
747 69. Chartier C, Degryse E, Gantzer M, Dieterle A, Pavirani A, Mehtali M. 1996. Efficient generation
748 of recombinant adenovirus vectors by homologous recombination in Escherichia coli. J Virol
749 70:4805–4810.
750 70. Gugliesi F, Mondini M, Ravera R, Robotti A, de Andrea M, Gribaudo G, Gariglio M, Landolfo S.
751 2005. Up-regulation of the interferon-inducible IFI16 gene by oxidative stress triggers p53
752 transcriptional activity in endothelial cells. J Leukoc Biol 77:820–829.
753 71. Woodward JJ, Iavarone AT, Portnoy DA. 2010. c-di-AMP secreted by intracellular Listeria
754 monocytogenes activates a host type I interferon response. Science 328:1703–1705.

755

756 **FIGURE LEGENDS**

757 **FIG 1** Inhibition of IFN-β response by HCMV pp65. (A) HFFs were infected at an MOI of 1 with
758 wild-type, v65Rev or v65Stop viruses and processed by RT-qPCR. Kinetics analysis results for IFN-β
759 mRNA expression following HCMV- versus mock-infection were normalized to those for GAPDH
760 expression and are shown as mean fold changes ± SD (**, $P$<0.01; one-way ANOVA followed by
761 Bonferroni's post-tests; for comparison of treated versus untreated cells). (B) HFFs were transduced
762 with AdVLacZ (black bar) or AdVpp65 (grey bar) at an MOI of 50. Afterwards, cells were infected

763 with v65Stop (MOI of 1). Following a further 6 hpi, IFN-β mRNA expression was normalized to that
764 of GAPDH and is shown as a mean ± SD fold change (**, $P$<0.01; unpaired t-test; for comparison of
765 AdVpp65- versus AdVLacZ-transduced cells) (left panel). The efficiency of pp65 overexpression was
766 analyzed by Western blot with anti-pp65 monoclonal antibody; α-Tubulin was included as a loading
767 control. Experiments were repeated at least three times and one representative result is shown (right
768 panel). (C) HFFs were infected with wild-type, v65Rev or v65Stop at an MOI of 1 or stimulated with
769 poly(I:C) (4 µg/mL). Supernatants were collected at the indicated times post infection and assessed by
770 ELISA for IFN-β production. Results are shown as a mean ± SD fold change (*, $P$<0.05; one-way
771 ANOVA followed by Bonferroni's post-tests; for comparison of wild-type/v65Rev- versus
772 v65Stop/poly(I:C)-treated cells).
773
774 **FIG 2** Generation of specific gene knockout cell lines by CRISPR/Cas 9-mediated genome editing.
775 Knockout (KO) gene variants in HFFs for cGAS (cGAS KO), STING (STING KO), and IFI16 (IFI16
776 KO), were generated using CRISPR-Cas 9 technology. The efficiency of IFI16, cGAS, and STING
777 protein depletion was assayed by (A) RT-qPCR for cGAS, STING, IFI16, and the housekeeping gene
778 GADPH; data are shown as mean fold changes ± SD (***, $P$<0.001 two-way ANOVA followed by
779 Bonferroni's post-tests; for comparison of KO- versus WT cells). (B) Western blot analysis for cGAS,
780 STING, IFI16, and Vinculin, as loading control. (C-D) TIDE analysis to quantify indel frequencies and
781 composition, by using PCR amplicons spanning the sgRNA target sites for sanger sequencing and
782 subsequent analysis by the TIDE software (http://tide.nki.nl).
783
784 **FIG. 3** The cGAS/STING axis mediates IFN-β production during HCMV infection. (A) Control HFFs
785 (WT), cGAS KO, STING KO, IFI16 KO were infected with wild-type, v65Rev or v65Stop viruses at
786 an MOI of 1. Six hours later, IFN-β mRNA expression was processed by RT-qPCR. The values were

normalized to GAPDH mRNA and plotted as a fold induction over WT HFFs. RT-qPCR data are shown as mean fold changes ± SD (*, $P<0.05$; ***, $P<0.001$ two-way ANOVA followed by Bonferroni's post-tests; for comparison of KO- versus WT cells). (B) HFFs WT, cGAS KO, STING KO or IFI16 KO were infected with wild-type, v65Rev or v65Stop viruses at an MOI of 1. Supernatants from the cells were collected at 24 hpi and analyzed by IFN-β ELISA. Results are shown as a mean ± SD fold change (*, $P<0.05$; ***, $P<0.001$ two-way ANOVA followed by Bonferroni's post-tests; for comparison of KO versus WT cells). (E-F) WT, cGAS KO, STING KO, and IFI16 KO HFFs were transfected with poly(I:C). IFN-β mRNA modulation was assessed by RT-qPCR 6 hpt (C) or IFN-β ELISA assay 24 hpt (D). Results are shown as a mean ± SD fold change (***, $P<0.001$ two-way ANOVA followed by Bonferroni's post-tests; for comparison of poly(I:C)-transfected cells versus untransfected cells).

**FIG 4** HCMV pp65 inhibits cGAS activity. (A) HFFs were infected with wild-type, v65Rev or v65Stop at an MOI of 1 for 24 h. Extracts from the infected cells were prepared, DNase- and heat-treated, and incubated with permeabilized HFFs for 6 h. IFN-β RNA induction was analyzed by RT-qPCR and normalized to GAPDH and is shown as a mean fold change ± SD following HCMV- versus mock-infection (**, $P<0.01$, one-way ANOVA followed by Bonferroni's post-test). (B) HFFs were electroporated with pp65 Halo-WT or left untransfected and then infected with v65Stop at an MOI of 1 for 24 h. cGAMP was harvested at 24 hpi and assayed on HFFs. IFN-β mRNA induction was measured in HFFs at 6 hpi by RT-qPCR (***, $P<0.001$ one-way ANOVA followed by Bonferroni's post-test, for comparison of v65Stop-HaloTag-transfected cells versus v65Stop-untransfected cells). (C) Cells were transduced as described in (B) and 24 h later transfected with poly(dA-dT) (4 μg/mL) for 24 h and assayed on HFFs. IFN-β mRNA induction was measured in HFFs at 6 h by RT-qPCR (***, $P<0.001$ one-way ANOVA followed by Bonferroni's post-test, for comparison of poly(dA-dT)- HaloTag-

811 transfected cells versus poly(dA-dT)-untransfected cells). (D) WT, cGAS KO, STING KO, and IFI16
812 KO HFFs were infected with wild-type, v65Rev or v65Stop at an MOI of 1. cGAMP was harvested at
813 24 hpi and assayed on HFFs. IFN-β mRNA induction was measured in HFFs at 6 hpi by RT-qPCR
814 (***, $P<0.001$; two-way ANOVA followed by Bonferroni's post-test). (E) HFFs were transfected with
815 synthetic 2'3'-cGAMP, 2'3'-cGAMP control (2 μg/mL), or HFFs were electroporated with pp65 Halo-
816 WT and then transfected with 2'3'-cGAMP. IFN-β mRNA induction was analyzed by RT-qPCR at the
817 time points indicated, and normalized to GAPDH. The experiment was repeated six times and no
818 statistically significant differences by unpaired t-test analysis were observed between cells transfected
819 with cGAMP alone versus cGAMP plus pp65 Halo-WT.
820
821 **FIG 5** pp65/cGAS interaction. (A) HFFs were infected with wild-type, v65Rev or v65Stop viruses
822 (MOI of 1) or left uninfected (mock) and subjected to IIF at 2 hpi. pp65 (green)/cGAS (red) were
823 visualized using primary antibodies followed by secondary antibody staining in the presence of 10%
824 HCMV-negative human serum. Nuclei were counterstained with TO-PRO-3 (blue). Images were
825 generated by confocal microscopy; the far right hand picture shows a 3D image reconstruction using
826 the confocal Z stacks. Digitally reconstructed 3D images were generated for at least 5 fields per
827 condition; representative images are shown. (B) A Proximity Ligation Assay (PLA) was performed to
828 detect protein-protein interactions using fluorescence microscopy. The signal was detected as distinct
829 fluorescent dots in the Texas Red channel when cells reacted with the indicated pairs of primary
830 antibodies followed by PLA to assess the interactions between pp65/cGAS. (C) Co-
831 immunoprecipitation from virus-infected or mock-infected cell lysates. HFFs were infected with wild-
832 type, v65Rev or v65Stop viruses (MOI of 1) and harvested at 2 hpi. Immunoprecipitations were
833 performed using antibodies against pp65 or without antibody as negative control (CTRL).
834 Immunoprecipitated proteins were detected by Western blot analyses using antibodies against pp65,

835 cGAS, and STING. Non-immunoprecipitated whole-cell extracts (Input) were immunoblotted using
836 anti-pp65, anti-cGAS, and anti-STING antibodies. (D) Immunoprecipitation was performed as
837 described in (C) except that the samples were split in two, and half were treated with benzonase (1
838 U/µL) for 2 h on ice followed by immunoprecipitation using antibodies against pp65 (left panel). The
839 mock cell lysate used in the IP depicted in the left panel was run onto an ethidium bromide-stained
840 (0.8%) agarose gel. Lane 1: IP in the absence (-) of benzonase; lane 2: IP in the presence (+) of
841 benzonase (right panel). (E) Mapping the region of pp65 required for its interaction with cGAS. Wild-
842 type pp65 (pp65 Halo-WT) and serial deletion mutants of pp65 (pp65 Halo-ΔN, pp65 Halo-ΔC) were
843 used to immunoprecipitate lysates of HFFs transiently expressing pp65 HaloTag. Interaction was
844 detected by Western blot analysis using antibodies against cGAS.
845
846 **FIG 6** STING undergoes proteasome degradation. (A) HFFs were infected with wild-type, v65Rev or
847 v65Stop viruses at an MOI of 1. Lysates were prepared at the indicated time-points and subjected to
848 Western blot analysis for pp65, cGAS, STING, and α-Tubulin. (B) Western blot analysis for STING in
849 cells transfected with poly(dA-dT) (4 µg/mL) at the indicated time-points. Lysates were also stained for
850 α-Tubulin as a loading control. (C) HFFs infected with wild-type, v65Rev and v65Stop viruses (MOI
851 of 1) were treated with MG132 or DMSO. Cells were harvested at 6 and 24 hpi and processed for
852 Western blot analyses with antibodies against STING. Lysates were also stained for pp65 and with α-
853 Tubulin as a loading control. (D) Co-immunoprecipitation from virus-infected or mock-infected cell
854 lysates. HFFs were infected with wild-type, v65Rev, or v65Stop viruses (MOI of 1) and harvested at 2
855 hpi. At the indicated time points, total cell protein extracts were immunoprecipitated for ubiquitin and
856 stained with anti-STING antibodies. Immunoprecipitation of ubiquitin-conjugated proteins was
857 performed using the UbiQapture-Q Kit (Enzo LifeScience). (E) Cells were infected as described in (D).
858 Immunoprecipitations were performed using antibodies against Ubiquitin-K48-specific.

859 Immunoprecipitated proteins were detected by Western blot analyses using antibodies against STING.
860 Non-immunoprecipitated whole-cell extracts (Input) were immunoblotted using anti-STING and with
861 α-Tubulin antibodies as a loading control.
862
863 **FIG 7** Model depicting the proposed functional role of pp65 modulation of IFN-β activity during
864 HCMV infection.

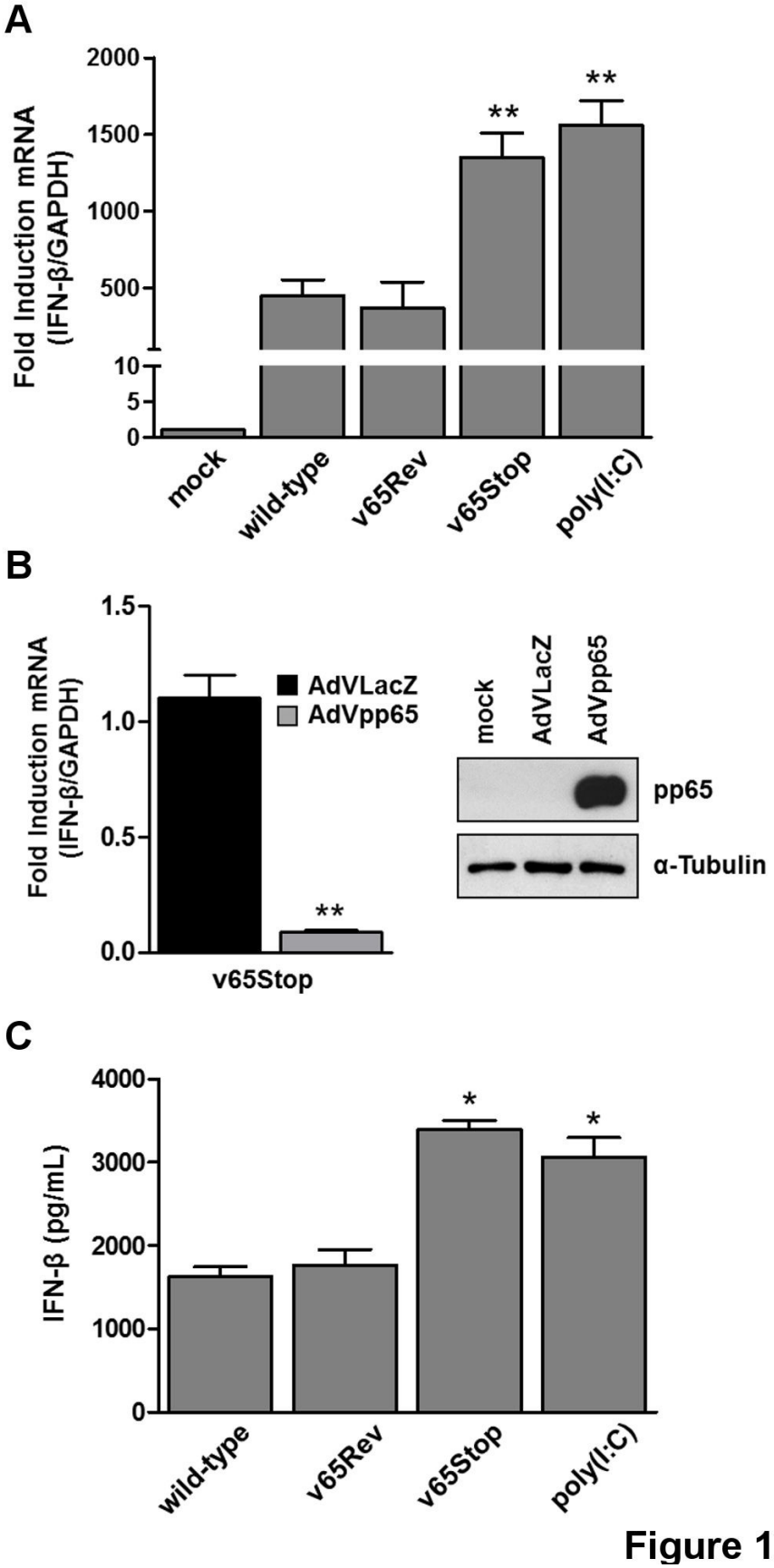


**Figure 1**

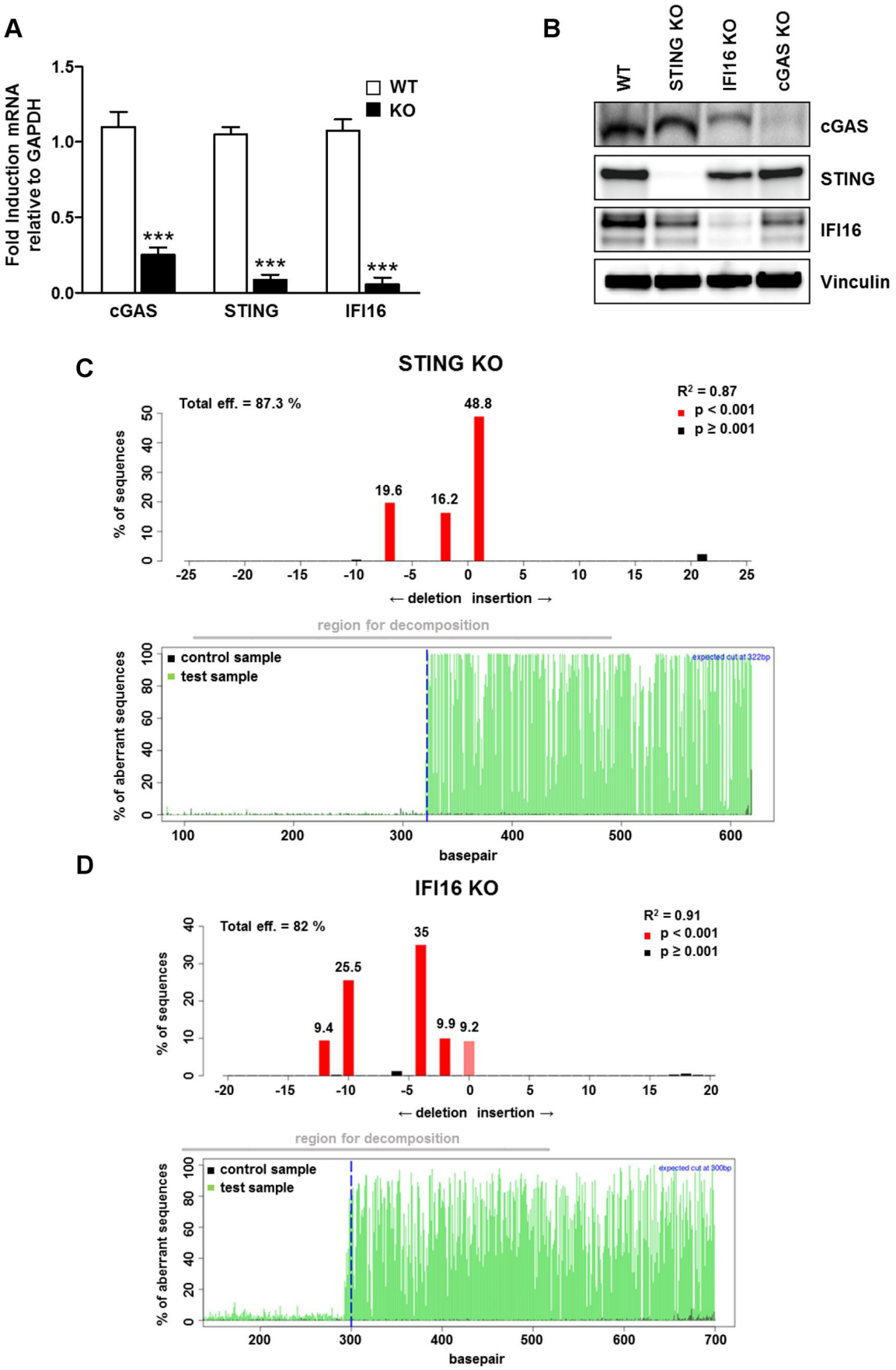


Figure 2

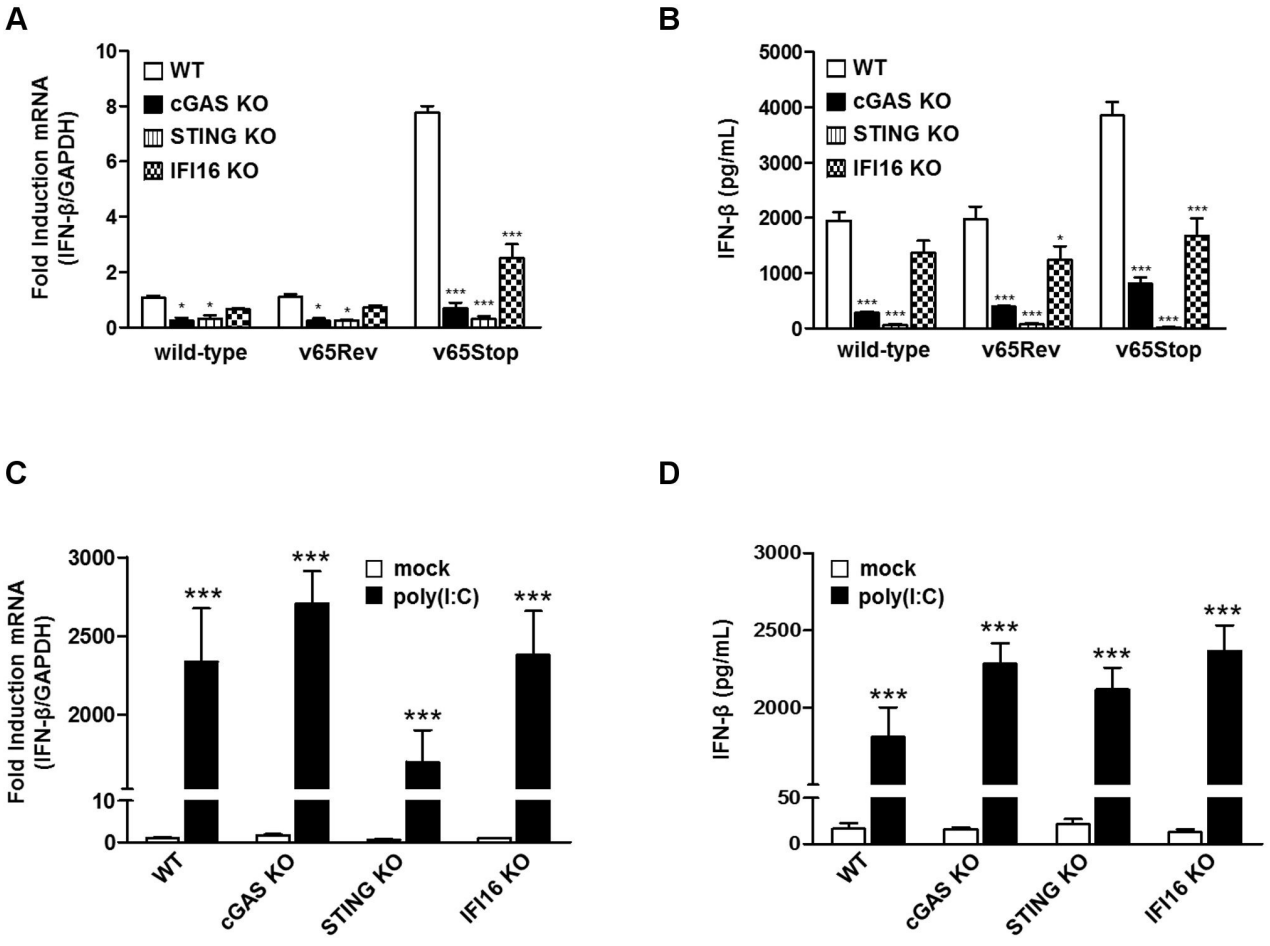


Figure 3

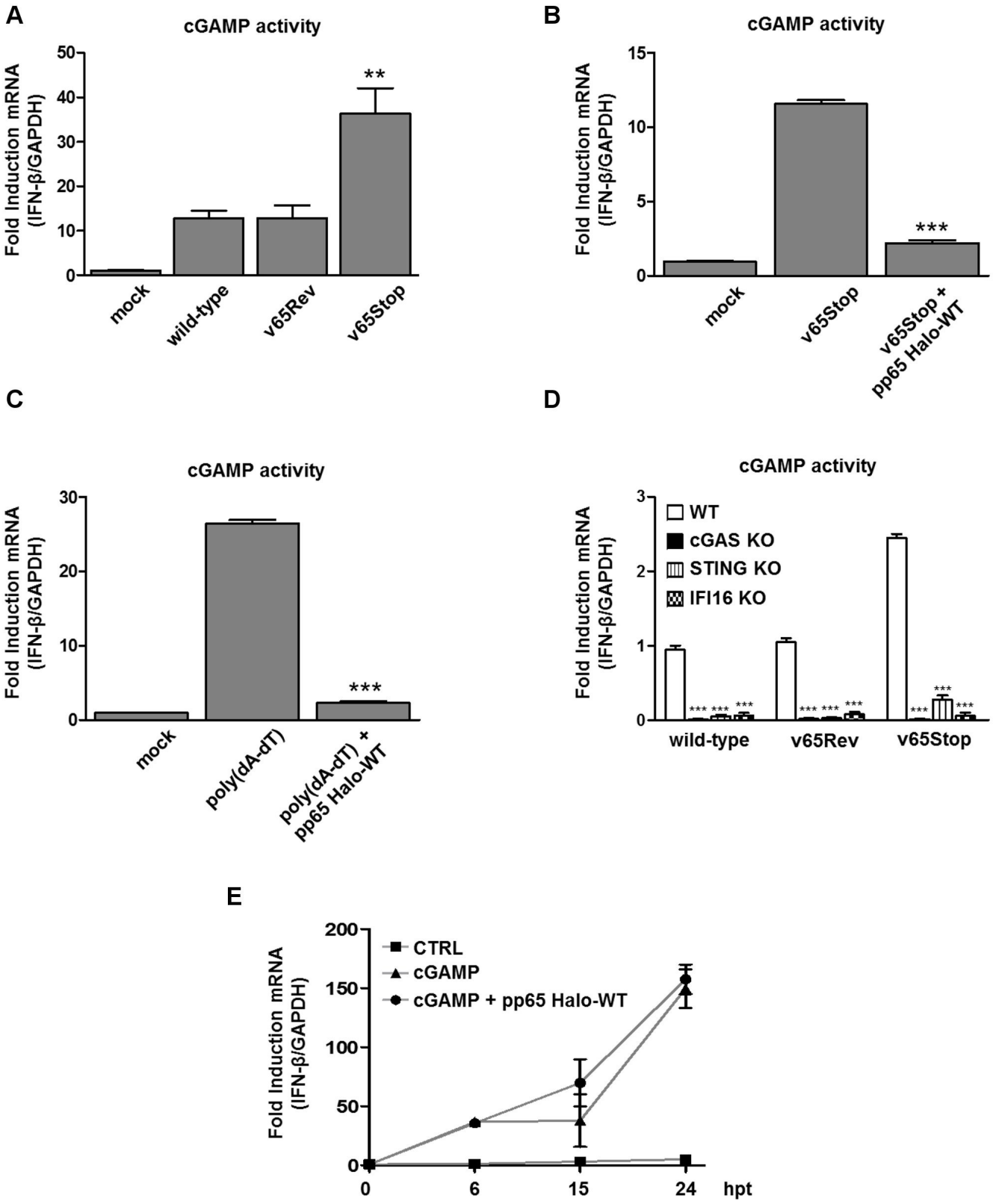


**Figure 4**

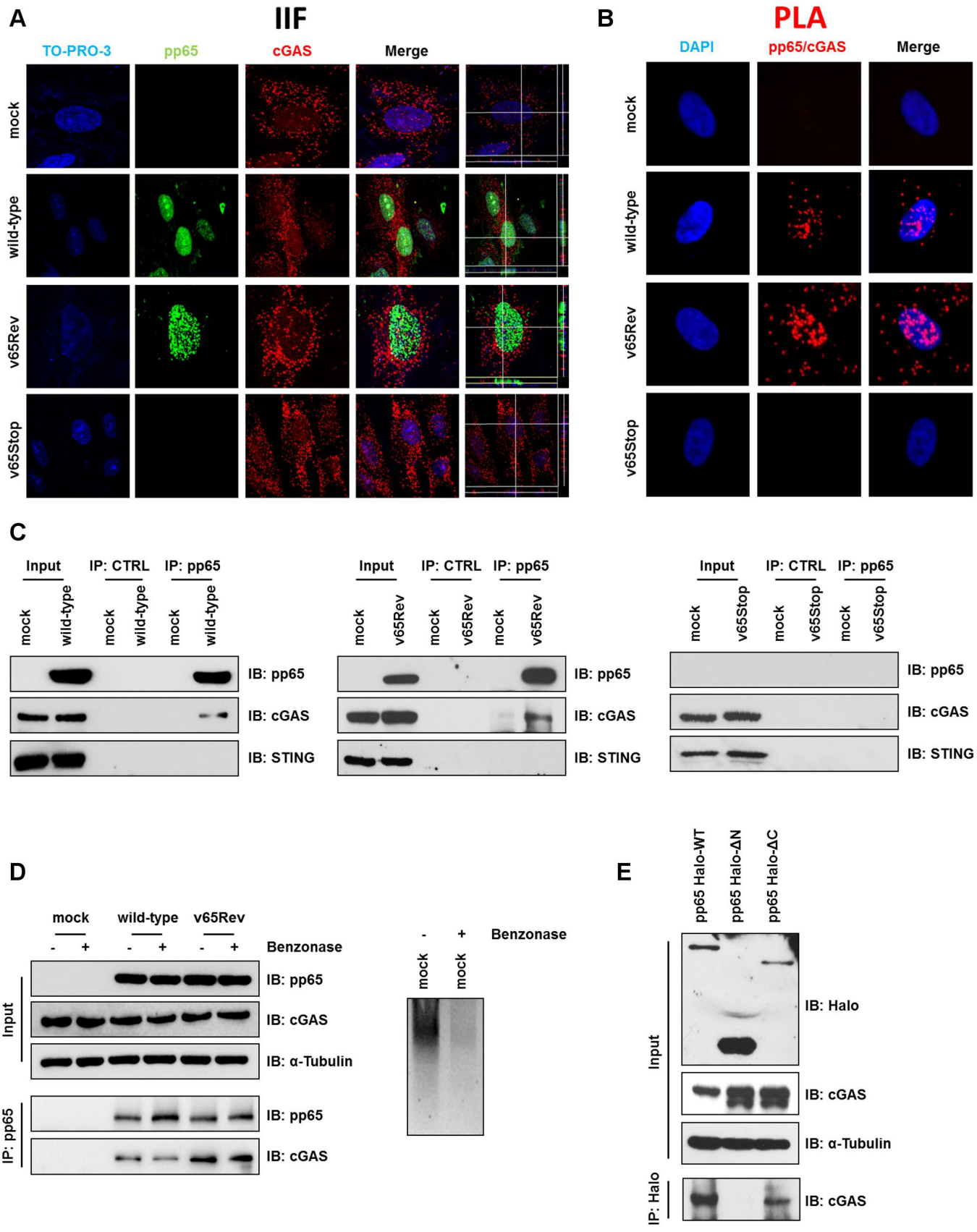


**Figure 5**

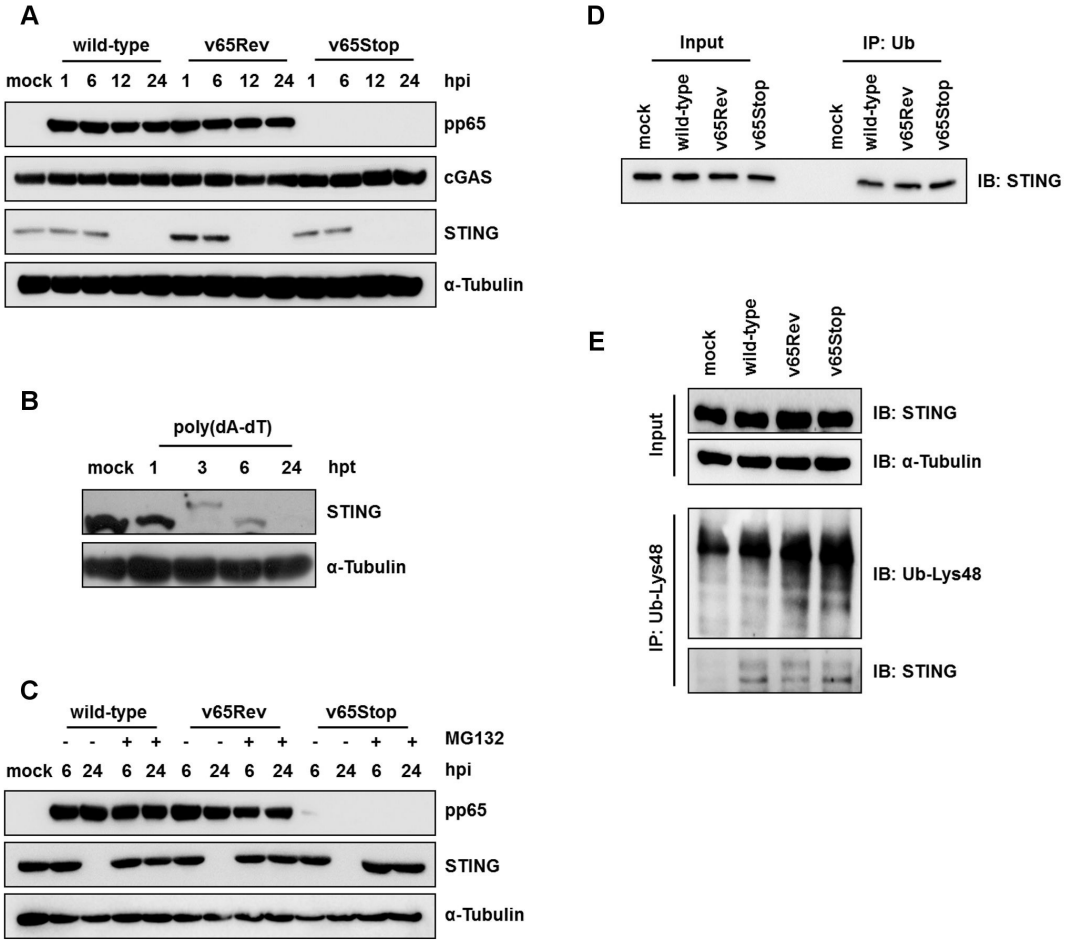


**Figure 6**



Journal of Virology

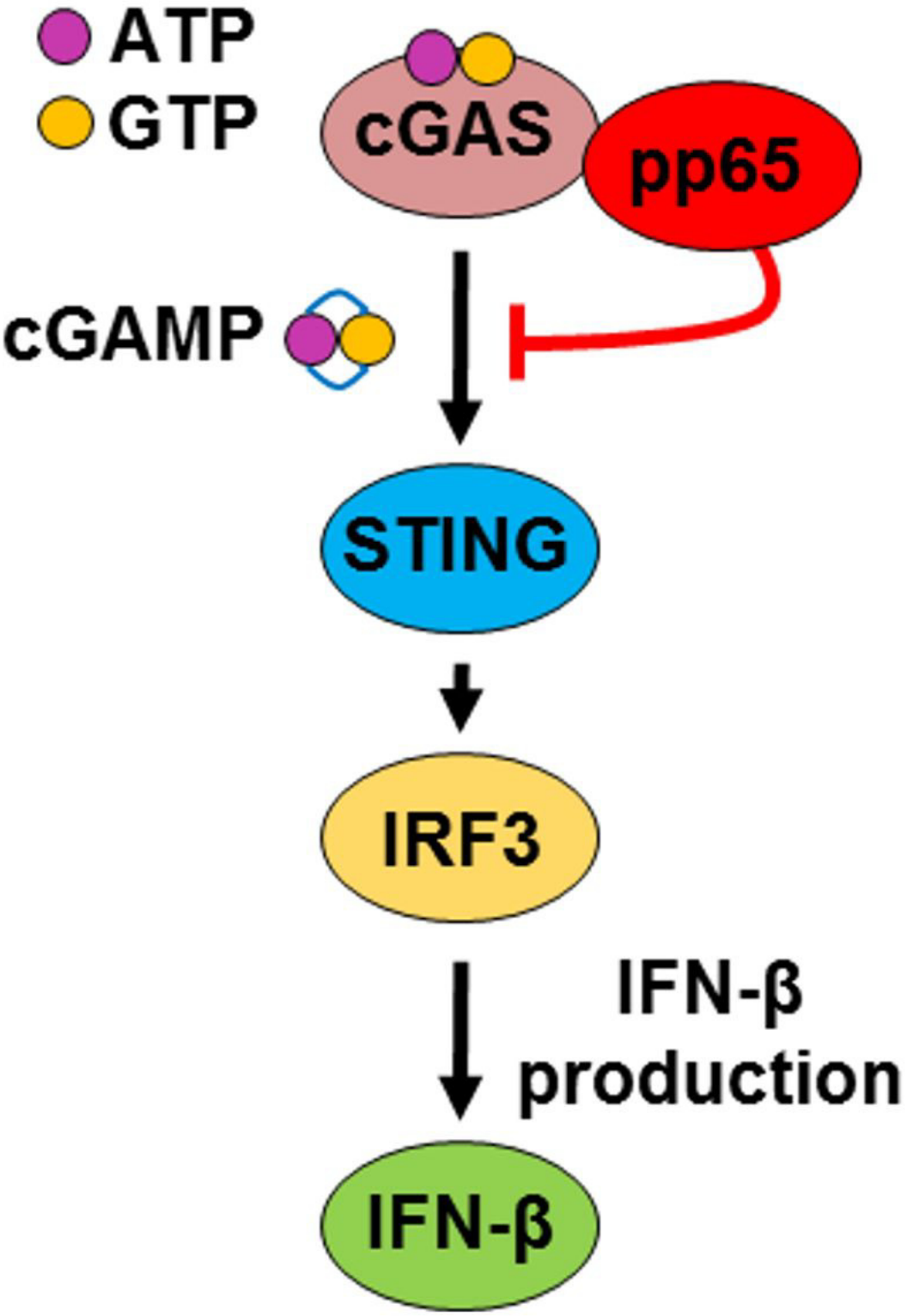


Figure 7